

pubs.acs.org/ac Article

Quantification of the Photon Absorption, Scattering, and On-Resonance Emission Properties of CdSe/CdS Core/Shell Quantum Dots: Effect of Shell Geometry and Volumes

Joanna Xiuzhu Xu, Yucheng Yuan, Muqiong Liu, Shengli Zou, Ou Chen, and Dongmao Zhang*



Cite This: *Anal. Chem.* 2020, 92, 5346–5353



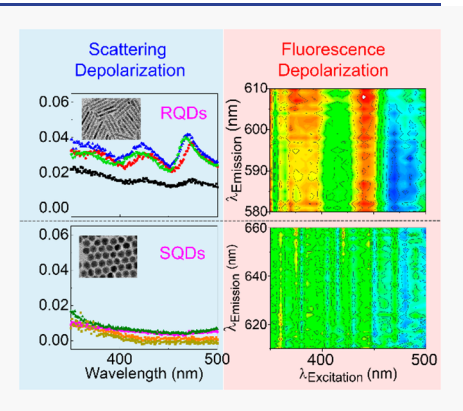
ACCESS

III Metrics & More



Supporting Information

ABSTRACT: Reliable quantification of the optical properties of fluorescent quantum dots (QDs) is critical for their photochemical, -physical, and -biological applications. Presented herein is the experimental quantification of photon scattering, absorption, and on-resonance-fluorescence (ORF) activities of CdSe/CdS core/shell fluorescent QDs as a function of the shell sizes and geometries. Four spherical QDs (SQDs) with different diameters and four rod-like QDs (RQDs) with different aspect ratios (ARs) have been analyzed using UV—vis, fluorescence, and the recent polarized resonance synchronous spectroscopic (PRS2) methods. All quantum dots are simultaneous absorbers and scatterers in the UV—vis wavelength region, and they all exhibit strong ORF emission in the wavelength regions where the QDs both absorb and emit. The absorption and scattering cross-sections of the CdS shell are linearly and quadratically, respectively, proportional to the shell volume for both the SQDs and RQDs. However, the effects of CdS shell coating on the core optical properties are different between SQDs and RQDs. For RQDs, increasing the CdS shell volume through the length elongation has no effect



on either the peak wavelength or intensity of the CdSe core UV—vis absorption and ORF, but it reduces the QD fluorescence depolarization. In contrast, increasing CdS shell volume in the SQDs induces red-shift in the CdSe core peak UV—vis absorption and ORF wavelengths, and increases their peak cross-sections, but it has no effect on the SQD fluorescence depolarization. The RQD ORF cross-sections and quantum yields are significantly higher than their respective counterparts for the SQDs with similar particle sizes (volumes). While these new insights should be significant for the QD design, characterization, and applications, the methodology presented in this work is directly applicable for quantifying the optical activities of optically complex materials where the common UV—vis spectrometry and fluorescence spectroscopy are inadequate.

INTRODUCTION

Fluorescent quantum dots (QDs) have demonstrated their diverse applications in bioimaging, ¹⁻³ lasing, ^{4,5} optical devices, ^{6,7} and energy conservations ⁸⁻¹² owing to their exceptional fluorescence properties. Core/shell fluorescent QDs exhibit enhanced photoluminescence quantum yields (QY), lower oscillator strength for the radiative transitions, and longer radiative lifetime due to the introduction of shell that effectively reduces electron-hole spatial overlap and reduction of trap states. ^{13–15} The QD optical properties can be tuned by different shell structures and geometries. ^{16–19} A systematic quantitative understanding of the correlations between QD shell structures and its resultant absorption, scattering, and fluorescence activities is key to rationalization of their synthetic design and optical applications. As an example, reliable quantification of QD absorption cross-section is important for evaluation of the QD fluorescence QY, 20 brightness, 21 number of excitons²² and the oscillator strength of the transitions.²³ However, a general literature practice for determining QD absorption activity is to assign the QD UV-vis extinction obtained directly with UV-vis spectrophotometers as its absorbance (or absorption extinction) spectrum. ^{24–26} The validity of this approach has not been systematically evaluated. In fact, both material light scattering and absorption contribute to its UV—vis extinction spectrum. ²⁷ For dissolved small molecular chromophores, their scattering cross-sections are usually negligibly small in comparison to their photon absorption cross-sections. ^{28,29} Therefore, their UV—vis extinction spectra can be taken as their absorption extinction (absorbance) spectrum. However, for nanoscale materials such as fluorescent QDs and molecular aggregates, the light scattering extinction contribution to the sample UV—vis extinction spectra may no longer be negligible. Indeed, one can approximate the QD UV—vis extinction spectrum as its absorbance spectra only when the ratio between the QD light

Received: January 2, 2020 Accepted: March 3, 2020 Published: March 3, 2020





scattering extinction and total extinction (or scattering-to-extinction ratio, SER) is negligibly small.

Herein we reported a series of fundamental optical constant spectra for QDs differing in their sizes and/or shapes. These spectra include (1) the OD UV-vis extinction, absorption extinction, and scattering extinction cross-section spectra. (2) The QD on-resonance fluorescence (ORF) emission crosssection and ORF OY spectra. Unlike the commonly measured Stokes'-shifted fluorescence (SSF) which is detected at wavelengths red-shifted from the excitation wavelength, ORF refers to the fluorescence emission occurring at the same wavelength as the excitation wavelength. 28,29 Furthermore, the ORF QY is obtained by dividing the QD ORF cross-section with its absorption cross-section at every excitation wavelength, 28 which is therefore the measure of absolute QY for the ORF emission. In contrast, the SSF QY is obtained by using external standards as references, therefore, the SSF are relative and their accuracy depending on the reference samples and similarity in the optical properties of the reference and the sample of interest. (3) Light scattering depolarization spectra and the total fluorescence depolarization spectra.²⁸

With the only exception of the QD extinction spectra, none of the aforementioned spectra are available before. One key learning from this work is that while all QDs exhibit intense light scattering, their UV—vis extinction remains totally dominated (>99%) by their photon absorption. While this observation offers a much needed justification to the literature practice in taking the QD UV—vis extinction spectrum as its absorbance spectra, the decomposition of the QD UV—vis extinction spectrum into its absorption and scattering component spectra provides a series of critical new insights to the effect of the shell volume and geometry on the QD optical properties.

The quantification of the QD optical properties was performed using combination of UV-vis, fluorescence, and the recently developed polarized resonance synchronous spectroscopic (PRS2) techniques. 28,30 PRS2 is similar to the conventional resonance synchronous spectroscopic (RS2) method. Both PRS2 and RS2 spectra are acquired using spectrofluorometers by setting the excitation and detection wavelengths identical while scanned synchronously. However, unlike the RS2 method that uses collimated nonpolarized light (or plane polarized light) for excitation and detection, PRS2 uses linearly polarized light for both excitation and detection. Such a change has profound impacts on improving the reliability of the data interpretation. First, PRS2 enables one to reliably separate the material ORF from light scattering in the detected signal. In contrast, RS2 attributes all detected signal to material light scattering, leading to a highly persistent literature practice of mistakenly labeling sample RS2 spectra as its resonance light scattering (RLS) spectrum. 31-34 Second. PRS2 measures the material light scattering and ORF fluorescence depolarization, which is critical to deduce the three-dimensional distribution of the scattered and ORF photons for the calculation of the sample light scattering and ORF cross-sections.²⁸ In contrast, the RS2 method only measures the photons propagating to the detector placed 90° relative to the excitation beam. Therefore, the spectra obtained with the RS2 measurements are instrument dependent and measurement specific, impossible to quantify the material fundamental optical constant spectra. Third, the PRS2 corrects the sample inner filter effect (IFE) introduced by the sample photon absorption, while the existing RS2 or "RLS" measurement either ignores the sample IFE or treats the light scattering and absorption the same in their sample IFE. Recent work has shown that for samples with a relatively low optical density (<1.5), only light absorption, but not light scattering introduces significant IFE.²⁷

There have been so far four variants of PRS2 methods differing in their general applicability and implementation complexity. The first is the direct PRS2 method that is applicable for all nonphotoluminescent materials and a subset of photoluminescent samples with zero light scattering depolarization but unity fluorescence depolarization in the wavelength region where the sample is ORF active.²⁸ The second method is a bandwidth-varied PRS2 (BV-PRS2) technique that is applicable to all samples including the samples that are simultaneous light absorbers, scatterers, and emitters under resonance excitation and detection conditions.³⁵ One drawback of the BV-PRS2 technique is tedious data analysis and processing. The third is the polarized anti-Stokes-shifted, on-resonance, and Stokes-shifted spectroscopic (PAOS) method that is also applicable to all samples.³⁰ The key advantage of PAOS method is that it enables direct visualization and separation of the light scattering and fluorescence contribution to the signal detected under resonance excitation and detection conditions. However, the spectral acquisition and processing for the PAOS-based PRS2 analysis with the existing commercial spectrofluorometer is very time-consuming. One complete PAOS spectrum is needed in order to extract the light scattering and fluorescence contribution to the resonance signal detected at each wavelength. The fourth method is the divide-and-conquer PRS2 technique that uses combination of the direct PRS2 and the PAOS methods.³⁰ This approach combines high efficiency, general applicability, and easy understanding. The divide-andconquer method first divides the UV-vis extinction spectrum into two regions based on the sample optical properties under the resonance excitation and detection conditions. The timeconsuming PAOS technique is necessary only to a narrow spectral wavelength region (<50 nm) where the samples are simultaneously photon absorbers, scatterers, and emitters, and the drastically more efficient direct PRS2 method is applied to the remaining UV-vis wavelength region where the samples are only simultaneously photon absorbers and scatterers, or scatterers only under the resonance excitation and detection condition.

■ EXPERIMENTAL SECTION

QD Syntheses and Characterizations. A total of eight CdSe/CdS core/shell fluorescent QDs, four spherical and four rod-shaped, are employed as the model QDs (Figure 1). All SQDs have the same spherical core (4.3 nm in diameter), but with varying shell thicknesses that result in QD diameters of 5.6 nm, 7.4 nm, 9.2 nm, and 10.8 nm, respectively. For the sake of discussion convenience, these SQDs are referred to as SQD5.6, SQD7.4, SQD9.2, and SQD10.8, respectively. The CdSe core used for the preparation of the rod-shaped QDs (RQDs) are also spherical, but with a smaller diameter (3.0 nm in diameter) for easy synthesis of long rods. The four RQDs all have the same width (4.4 nm) but with different lengths (Supporting Information (SI) Figure S1) that result in different aspect ratios (AR). These RQDs are referred to as RQD4.8, RQD9.3, RQD12.8, and RQD16.8, respectively, where the number specifies the aspect ratio of the RQDs. Detailed syntheses and molarity quantifications are described

Analytical Chemistry Article pubs.acs.org/ac

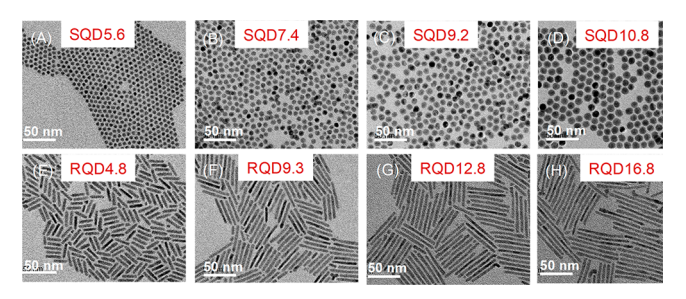


Figure 1. TEM images (A) SQD5.6, (B) SQD7.4, (C) SQD9.2, (D) SQD10.8, (E) RQD4.8, (F) RQD9.3, (G) RQD12.8, and (H) RQD16.8.

in the Supporting Information. The QD morphology is characterized by transmission electron microscopy (TEM) measurements, which were performed on a JEOL 2100F operated at 200 kV. The QDs were dispersed in hexane after purification, then drop cast on a 300-mesh copper TEM grid and dried at ambient condition before TEM measurements. The ligand binding on QD surface was characterized by thermal gravimetric analysis (TGA). (Figure 2 and SI Figure

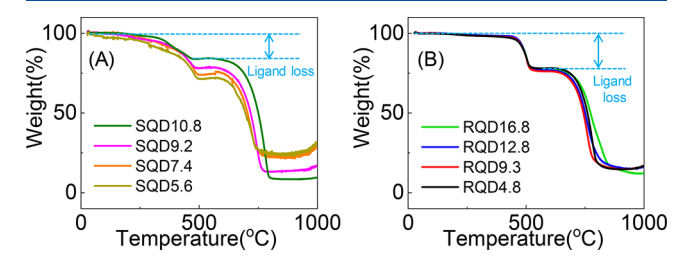


Figure 2. TGA thermograms of (A) SQDs and (B) RQDs. The weight loss range highlighted with blue dashed lines are ligand loss percentages for SQD10.8 in (A) and RQD16.8 in (B) as examples. The TGA thermograms of the cores are presented in SI Figure S2.

S2) The QD molarity was calculated with information obtained with TEM and TGA analysis (SI Table S1 and Table S2). The QD lifetime measurements were performed on an Edinburgh Instruments Fluorescence Spectrometer FS5. QDs were dispersed in hexane for measurements. The fluorescence lifetimes were measured with excitation at 360 nm, with an average acquisition time of 15 min and the sample optical density at 365 nm of 0.1.

UV-vis, Fluorescence, PRS2, and PAOS spectral Acquisitions. UV-vis, SSF and PRS2 spectra of the QDs are showed in SI Figure S3, and PAOS spectra are shown in SI Figure S4. The UV-vis extinction spectra were measured with a Thermo Scientific Evoltion 300 UV-vis spectrometer, and the SSF, fluorescence excitation, PRS2, and PAOS spectra were acquired with a Horiba FluoroMax-4 spectrofluorometer equipped with excitation and detection linear polarizers. Detailed PRS2 and PAOS spectral acquisition and analysis has been demonstrated before. 30 Unless indicated otherwise, all the spectrofluorometer-based spectra were acquired with an intergration time of 0.3 s, and a slit width of 2 nm for both the excitation and detection monochromators. The normalized spectra were used where the signal intensity was normalized by the signal from the sample detector and reference detector (S1/R1) to eliminate light source fluctuations.

Computational Simulations. The QD scattering depolarization spectra were computationally simulated by the Kramers-Kronig transformation method^{37,38} combined with the discrete dipole approximation (DDA) method. 39,40 Kramers-Kronig transformation method was used to calculate the index of refraction of QDs, with the experimentally measured absorption spectra, concentrations, and volumes of the QDs. Since the index of refraction of the QD is significantly different from its environment, herein we consider the wavelength change of the incident light due to the index of refraction of QD itself instead of pure solvent in the Kramers-Kronig transformation method. Discrete dipole approximation (DDA) method was then used to calculate the scattering depolarization spectra based on the QD geometric parameters and the obtained index of refractoin of QD.

RESULTS AND DISCUSSION

Quantification of the QD Optical Spectra. The TEM images of the CdSe/CdS core/shell QDs are shown in Figure 1. Based on the structural analyses of seeded-grown QDs performed in previous works, 16,41 the CdSe cores are located at the center in SQDs while at one end in the RQDs as depicted by the structural diagram (SI Figure S1). The width of all RQDs are essentially the same based on their TEM images (Figure 1) and the thermal gravimetric analysis (TGA) (Figure 2). The percentage of mass loss due to the ligand evaporation in the TGA thermograms are approximately the same for all RQDs (Figure 2B), which is consistent with the fact that the surface-to-volume ratios of the used RQDs are very similar due to their relatively large aspect ratios (SI Table S1). In contrast, the ligand evaporation-induced mass loss for the SQDs decreases with increasing QD diameter (Figure 2A), which is again consistent with the fact that for SQDs, their surface-tovolume ratios decrease with increasing particle sizes (SI Table

The shell geometry has enormous impact on the QD fluorescence depolarization or fluorescence anisotropy. Fluorescence depolarization and anisotropy can be readily converted into each other. 28 We choose to use fluorescence depolarization instead of anisotropy because depolarization is far more commonly used in light scattering literatures. Currently fluorescence depolarization or anisotropy has been mostly investigated using a single excitation or emission wavelength. We devised in this work a total fluorescence depolarization method to probe how the fluorescence depolarization varies as a function of the excitation and detection wavelengths (Figure 3A and B, and SI Figure S5 for their three-dimensional plots). Evidently the RQD fluorescence depolarization depends strongly on the RQD sizes and the excitation wavelengths (Figure 3C), whereas the SQDs have near unity fluorescence depolarization regardless of the SQD sizes and the excitation and detection wavelengths (Figure 3D).

The difference between RQDs and SQDs in their fluorescence depolarization is most likely due to rotational diffusion rate. Fluorescence depolarization is a function of fluorophore rotational correlation time and the fluorescence lifetime. 42 When the fluorophore rotational correlation time is much shorter than its fluorescence emission lifetime, the fluorescence emission diploes can adopt any angle relative to the excitation polarization after fast fluorophore rotations. In this case, the fluorescence emission is isotropic, which results in unity of fluorescence depolarization ($P^F = 1$). In contrast, if the fluorophore rotational correlation time is longer than fluorescence lifetime, the propagation of the emitted photons will be anisotropic $(P^F \neq 1)$. Since RQDs and SQDs have

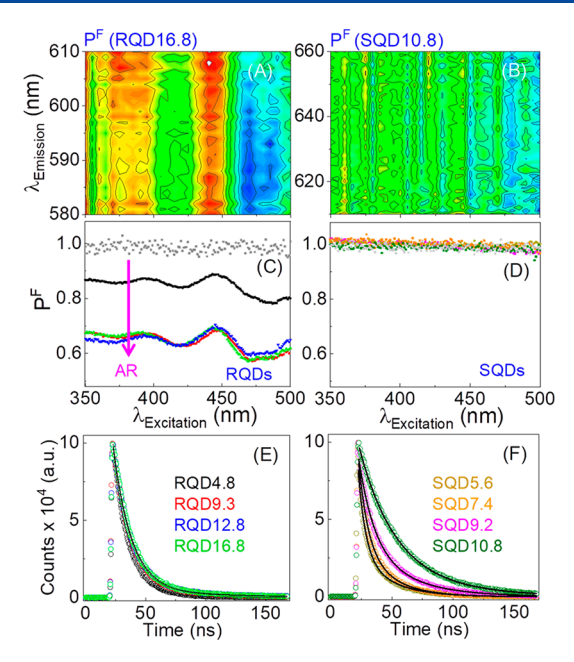


Figure 3. (A) and (B) show example total fluorescence depolarization (P^F) spectra of RQD16.8 and SQD10.8. (C) and (D) show fluorescence excitation depolarization spectra of SQDs and RQDs. The polarized fluorescence excitation spectra used for quantification of depolarization (P^F) is presented in SI Figure S5. (E) and (F) are fluorescence lifetime data of SQDs and RQDs, respectively. The circles are experimental data and the black traces are exponential fitting, which follows the two-exponential decay model (SI Tables S3 and S4).

similar fluorescence lifetimes (Figure 3E and F), the fact that fluorescence depolarizations of RQDs, especially the ones with large aspect ratios, deviate significantly from unity strongly suggests that (1), RQDs have longer rotational correlation time than SQDs, and (2) the rotational correction time of RQDs are longer than their respective fluorescence lifetime

The scattering depolarizations of both RQDs and SQDs are negligibly small at the QD emission wavelength region, which is manifested by the fact that no observable light scattering signal in the PAOS VH spectra obtained with the QDs (Figure 4R–U, and SI Figure S4). Since the fluorescence depolarizations of SQDs are unity, the efficient PRS2 method is directly applicable for decomposition of the SQD PRS2 spectra into their scattering and ORF component spectra, and subsequently the SQD UV–vis extinction spectra into their absorption and scattering extinction component spectra.(SI Figure S6)²⁸ In contrast, the PAOS spectra is necessary for quantifications of RQD light absorption, scattering, and ORF activities in its ORF active region because the RQD fluorescence depolarization is strongly excitation wavelength dependent (Figure 3).

The wavelength region where PAOS analysis is necessary can be readily identified by comparing UV—vis, SSF, and PRS2 VH spectra of individual RQD samples (Figure 4A—D). PRS2 VH refers to the PRS2 spectra taken under condition where the excitation polarization is vertical (V), but the detection polarization is horizontal (H) to the plane defined by the excitation source, sample chamber, and the detector. Only the wavelength region where all three spectra overlap can ORF occur, and thereby PAOS spectral acquisitions are required. The PAOS VV spectra acquired in the ORF-active wavelength region contain both light scattering, and anti-Stokes-shifted fluorescence, on-resonance fluorescence, and Stokes-shifted

fluorescence (Figure 4E–H). In contrast, the PAOS VH spectra are dominated by the RQD fluorescence with relatively small light scattering contribution (Figure 4M–P). Using the method described in the PAOS publication,³⁰ the RQD PRS2 VV and PRS2 VH spectra are decomposed into their respective ORF and light scattering component spectra. (Figure 4I–L, and R–U).

Effect of Shell Sizes and Geometries on Shell Scattering and Absorption Cross-Sections. The UV-vis extinction spectral features of CdSe/CdS core/shell QDs below 500 nm are dominantly contributed from the CdS shell, whereas those above 500 nm are predominantly from the CdSe core. 16 It has been known that QD photon extinction increases with increasing shell volume, but the fractional contributions of the shell light scattering and absorption have not been investigated. By decomposition of the QD UV-vis extinction spectra into their absorption and scattering component spectra, this work enables us to systematically evaluate effects of shell size and geometry on the QD absorption and scattering activity. There are several notable observations. First, while all QDs exhibit relatively high scattering intensity in the wavelength region attributed to the CdS shell (Figure 5B and G), the QDs are predominant light absorbers in this wavelength region since their absorption cross-sections are 2 orders of magnitude higher than their scattering cross-sections (Figure 5B, C, F and G). Second, none of the QDs can be approximated as Rayleigh scatterers ($\sigma = a\lambda^{-4}$) (insets in Figure 5B and G, and SI Figure S9) as assumed in a recent work,²¹ despite they are all in the Rayleigh scattering size domain with dimensions significantly smaller than the excitation wavelengths from 300 to 800 nm. This observation is in sharp contrast to the small polystyrene nanoparticles (100 nm in diameter) and solvent molecules that can all be approximated as Rayleigh scatterers.²⁹ Instead, the wavelength dependence of SQD and RQD scattering cross-sections can be approximated with the equation of $\sigma = a\lambda^{-6}$ (SI Figure S9) where the fitting coefficient a increases quadratically with increasing particle sizes. Third, regardless of their geometry, the absorption cross-section of CdS shell on the SQD and RQD is linearly proportional to the shell volume, while their light scattering cross-section increases quadratically with the latter (Figure 5D and H).

Resonance light scattering that occurs in the wavelength region where the scatterers absorb is likely responsible for the deviation of QDs from being Rayleigh scatterers. All Rayleigh scattering cross-section equation ($\sigma = a\lambda^{-4}$) is applicable only to nonabsorbing materials with sizes significantly smaller than the excitation wavelengths. While the model QDs are in the Rayleigh scatterers' size domains, they are all strong light absorbers in the investigated wavelength regions. The fact that QD light scattering cross-section follows a wavelength dependence of $\sigma = a\lambda^{-6}$ suggests that the enhancement factor due to QD resonance light scattering decreases with increasing wavelength. The latter is consistent with the fact that the overall QD UV-vis absorption cross-sections decrease with longer wavelength (Figure 5C and H).

The most surprising observation is the remarkably small light scattering depolarization ($P^{\text{Sca}} < 0.1$) of the RQDs (Figure 5E). Earlier works performed with the rod-shaped (CS₂) and spherical shape (CCl₄) molecules, ²⁹ as well as the spherical and rod-shaped gold nanoparticles (AuNPs) ⁴⁴ revealed that light scattering depolarization is very sensitive to scatterers' shapes. While the spherical scatterers have

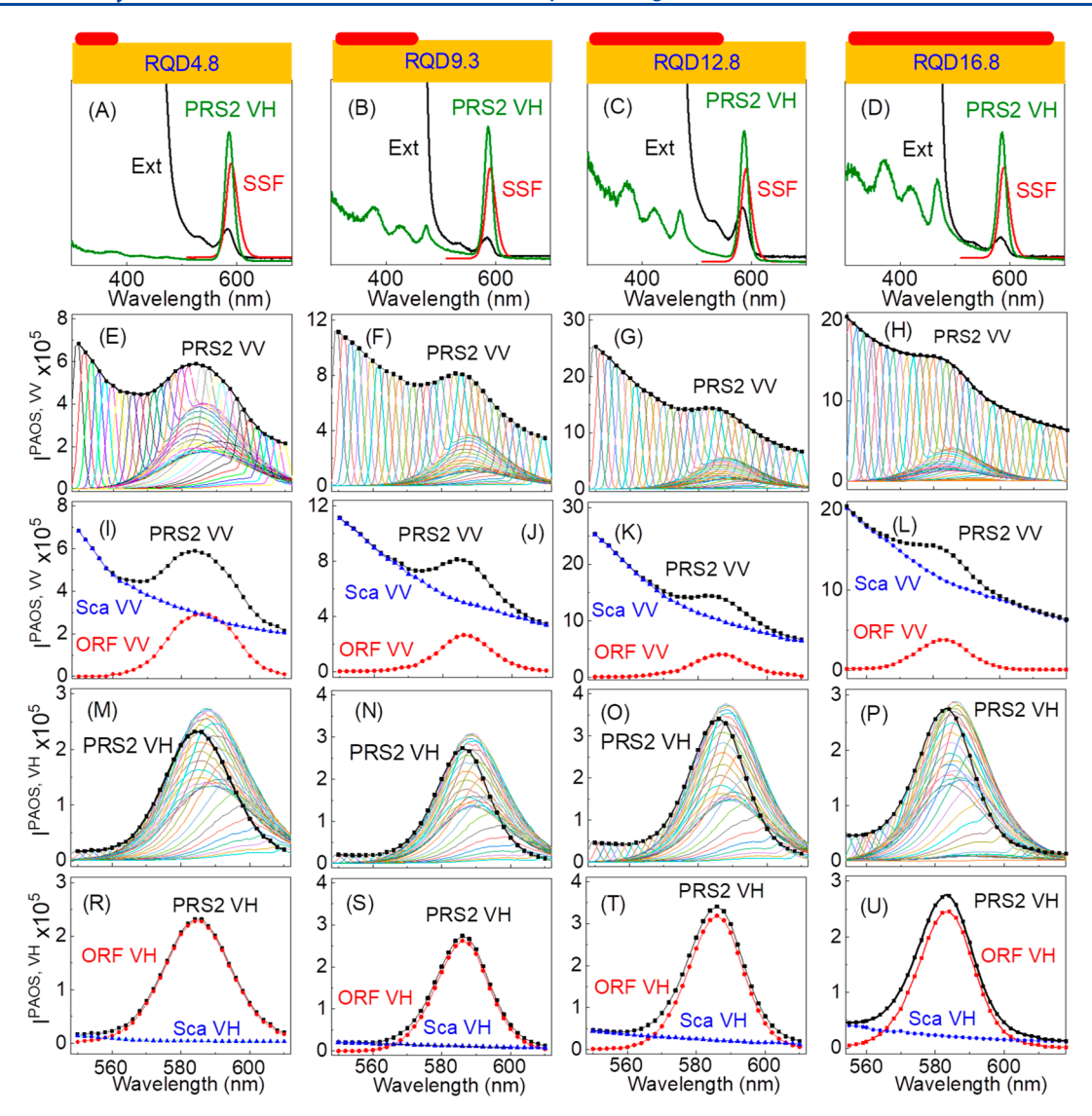


Figure 4. (1st row) (black) RQD UV—vis extinction (Ext) spectrum, (red) Stokes's Shifted Fluorescence (SSF) spectra, and (green) PRS2 VH spectra of (A) RQD4.8, (B) RQD9.3, (C) RQD12.8, (D) RQD16.8. (2nd row) PAOS VV spectra in the ORF-active region for (E) RQD4.8, (F) RQD9.3, (G) RQD12.8, (H) RQD16.8. (3rd row) Separation of scattering and ORF component in the PRS2 VV spectra with PAOS in the ORF-active wavelength region for (I) RQD4.8, (J) RQD9.3, (K) RQD12.8, (L) RQD16.8. (4th row) PAOS VH spectra in the ORF-active region for (E) RQD4.8, (F) RQD9.3, (G) RQD12.8, (H) RQD16.8. (5th row) Separation of scattering and ORF component in the PRS2 VH spectra with PAOS in the ORF-active wavelength region for (I) RQD4.8, (J) RQD9.3, (K) RQD12.8, (L) RQD16.8.

negligibly small light scattering depolarization ($P^{Sca} < 0.02$), the scattering depolarization of the rod-shaped scatterers can be as high as 0.5. As an example, the light scattering depolarization for the rod shaped CS₂ molecular is 0.5 from the 400 to 600 nm region, whereas the peak light scattering depolarization of the rod-shaped AuNP increases with increasing aspect ratio.^{29,44} The peak scattering depolarization of the gold nanorod with an aspect ratio of 3.2 is 0.45. While a similar trend is observed for the spherical and rod shaped QDs, that the light scattering depolarizations of the SQDs are smaller than that of the RQDs, and the peak RQD scattering depolarizations remain very small. The maximum light scattering depolarization is 0.04 for the RQD with an aspect ratio as large as 16.8. Computational simulations of the QD depolarizations agree well with the experimental results (SI Figure S10S).

Effect of Shell Sizes and Geometries on the Core Optical Properties. The QD spectral features above the 500

nm are due predominantly to the CdSe core. Earlier work established that shell coating enhances core UV—vis extinction and fluorescence emission. However, the enhanced UV—vis extinction can be due to the increased photon absorption, scattering, or both, while enhanced fluorescence emission can be due to the increased QD photon absorbance, fluorescence quantum yield, or both. The quantitative decomposition of the QD UV—vis extinction spectra into their absorption extinction (absorbance) and scattering extinction spectrum enabled us to pinpoint the physical origins of the increased core UV—vis and fluorescence intensity caused by the shell coating.

The shell coating enhances UV—vis absorption (Figure 6A and B) and ORF (Figure 6C and D) cross-sections of the CdS cores in both RQDs and SQDs QDs. However, despite their large difference in their shell volumes, all RQDs have approximately the same UV—vis cross-sections, ORF cross-sections, and ORF fluorescence quantum yields (Figure 6A, C, and E). In contrast, both the absorption and ORF cross-

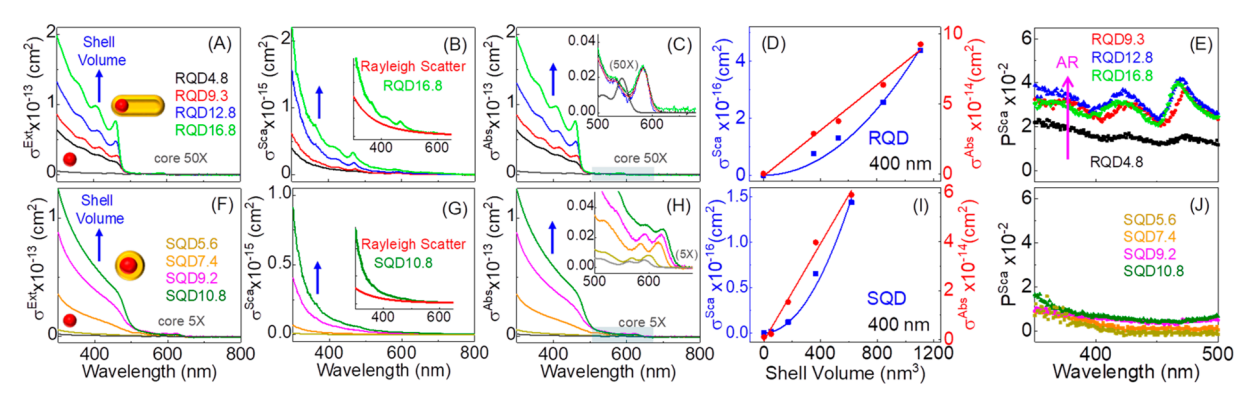


Figure 5. Optical constant spectra of (upper row) RQDs and (bottom row) SQDs and their respective cores. Magnified optical cross-section spectra of the cores are shown in SI Figure S7. (A, F), (B, G), and (C, H) are the QD total extinction, scattering, and absorption cross-section spectra, respectively. The insets in (C) and (H) are the zoomed-in in the longer wavelength region highlighted in blue in (C) and (H). (D) RQD (blue dots) scattering cross-sections and (red dots) absorption cross-sections as a function of shell volume at the excitation wavelength of 400 nm. (I) SQD (blue dots) scattering cross-sections and (red dots) absorption cross-sections as a function of shell volume at the excitation wavelength of 400 nm. Both scattering cross-sections are fitted quadratically and absorption cross-sections linearly. The data at other wavelengths are presented in SI Figure S8. Scattering depolarization spectra of (E) RQDs and (J) SQDs.

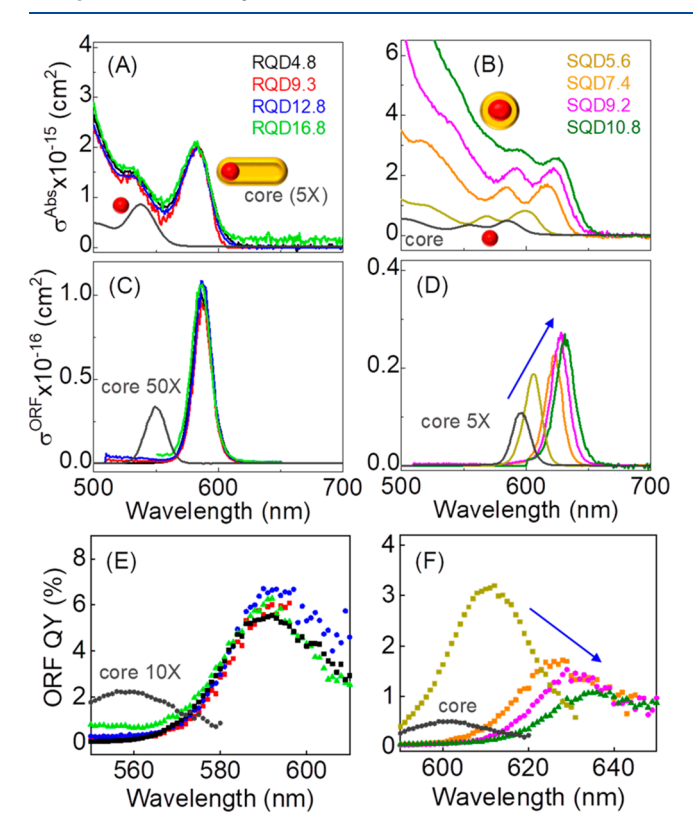


Figure 6. Optical properties in QD core region (500–700 nm). Absorption cross-section spectra of (A) RQDs and (B) SQDs. The gray curves represent data of the corresponding cores. ORF cross-section spectra of (C) RQDs and (D) SQDs. ORF QY spectra (ORF QY(λ) = $\sigma^{\text{ORF}}(\lambda)/\sigma^{\text{Abs}}(\lambda) \times 100\%$) of (E) RQDs and (F) SQDs.

sections of the CdS cores inside SQDs increase with increasing shell volume or shell monolayers. These results indicate that for RQDs, only the initial layer of CdS shell on the CdSe core is effective in enhancing the core photon absorption and on-resonance fluorescence. Once the CdS thickness on the RQDs surpasses a critical volume, further growing the CdS shell has no impact on either CdSe photon absorption or ORF activities. In contrast, absorption and ORF activities of the CdSe cores inside SQDs monotonically increases with increasing CdS shell

thickness (SI Figure S11). This trend is observed even when the shell thickness is as large as 3.8 nm in SQD10.8, which is equivalent to 9.6 monolayers of wurtzite CdS.

The difference in the shell volume dependence of the CdSe core optical properties between the RQDs and SQDs can be explained by their different shell geometric characteristics. For the RQDs, only the initial CdS shell grows three-dimensionally surrounding the CdSe (Figure 6A and SI Figure S1), further CdS elongation at one end of the rod is essentially zero dimensional. Therefore, only the initial three-dimensional CdS coating, which is the same for all RQDs with different aspect ratios, is effective in enhancing the CdSe core photon absorption and fluorescence activities, the subsequent CdS coatings that define the aspect ratio of the RQDs have no significant effect on the optical property of the core. As such, the CdSe core photon absorption and emission properties are the same in all RQDs despite of their difference in the aspect ratio and the shell volume.

The quantifications of the UV-vis absorption and ORF cross-section enable us to determine the QD ORF QY spectrum, which is the ratio between the QD ORF and absorption cross-section at the same excitation wavelengths. Comparing and contrasting the shell thickness dependence of the core UV-vis absorption cross-section, ORF cross-section, and ORF QY for the SQDs is revealing. For SQDs, the peak UV-vis absorption cross-section of the core increases linearly with further shell coating (Figure 6B and SI Figure S11), but the peak ORF cross-section increases most effectively with the initial CdS coating. Further increasing the CdS shell thickness has no significant effect on the RQD ORF cross-section (Figure 6D). The ORF QY of the CdSe core in SQDs increases significantly with the initial CdS coating. However, further increasing the thickness of the shell reduces the core ORF QY (Figure 6F). The data for SQDs indicate only the initial thin layer CdS shell coating are effective in enhancing both the core UV-vis photon absorption and ORF QY. Further increasing the shell thickness more effectively increases the SQD photon absorption, but less effectively increases their ORF emission due to the reduced ORF QY. While the fundamental mechanism for this experimental observation will be subjected to further investigation, the finding is important for optimizing QD fluorescence QY by design.

CONCLUSIONS

Fluorescent QDs are among the most optically complicated materials because they can simultaneously absorb, scatter, and emit photons under resonance excitation and detection conditions. This work quantified for the first time a series of fundamental optical constant spectra for a series of RQDs and SQDs that include their scattering, absorption and ORF crosssection spectra, scattering and ORF depolarization spectra, and ORF QY spectra. The QD shell scattering cross-section follows, empirically, $\sigma = a\lambda^{-6}$ where the value of coefficient a increases quadratically as a function of shell volume, whereas the shell absorption cross-section increases linearly with the shell volume for both the RQDs and SQDs. The shell geometry has significant impact on the QD fluorescence depolarization. All SQDs of different sizes all have negligible light scattering depolarization, but unity fluorescence depolarization in the entire UV-vis region. The RQD fluorescence and light scattering depolarization depends strongly on the shell size and the excitation wavelengths. Furthermore, varying CdS shell size has no significant effect on the core light absorption, scattering, and ORF fluorescence activities for the investigated RQDs, but increasing the shell thickness around core introduce systematic change in the optical property of the core in SQDs. Besides providing quantitative insights to the optical properties of CdSe/CdS core/shell nanoparticles, the methodology such as the total fluorescence depolarization measurements, PRS2, and PAOS techniques presented in this work should be important for a wide range of material characterization applications.

ASSOCIATED CONTENT

Supporting Information

The Supporting Information is available free of charge at https://pubs.acs.org/doi/10.1021/acs.analchem.0c00016.

QD synthesis and characterizations. UV—vis, SSF and PRS2 spectra of QDs. PAOS spectra of QDs in the ORF active region. As-acquired polarized fluorescence excitation spectra of QDs and example three-D total fluorescence depolarization spectra. QD fluorescence lifetime data. Optical cross-section spectra of cores. Example direct PRS2 method for quantification of SQD optical cross-section spectra. Curve fittings of QD scattering and absorption cross-sections as a function of shell volumes. Computational QD scattering depolarization spectra. Absorption cross-sections and peak wavelengths of the first absorption peak of SQDs as a function of shell thickness (PDF)

AUTHOR INFORMATION

Corresponding Author

Dongmao Zhang — Department of Chemistry, Mississippi State University, Mississippi State, Mississippi 39762, United States; orcid.org/0000-0002-2303-7338; Phone: (662) 325-6752; Email: Dongmao@chemistry.msstate.edu

Authors

Joanna Xiuzhu Xu — Department of Chemistry, Mississippi State University, Mississippi State, Mississippi 39762, United States Yucheng Yuan — Department of Chemistry, Brown University, Providence, Rhode Island 02912, United States; ocid.org/ 0000-0003-3935-0967

- Muqiong Liu Department of Chemistry, University of Central Florida, Orlando, Florida 32816, United States
- Shengli Zou Department of Chemistry, University of Central Florida, Orlando, Florida 32816, United States; orcid.org/0000-0003-1302-133X
- Ou Chen Department of Chemistry, Brown University, Providence, Rhode Island 02912, United States; ^⑤ orcid.org/ 0000-0003-0551-090X

Complete contact information is available at: https://pubs.acs.org/10.1021/acs.analchem.0c00016

Notes

The authors declare no competing financial interest.

ACKNOWLEDGMENTS

This work was supported by NSF funds (CHE 1151057) and (EPS-0903787) provided to D.Z. and ACS Division of Analytical Chemistry Summer Graduate Fellowship sponsored by the Society for Analytical Chemists of Pittsburgh provided to J.X. S.Z. thanks the Extreme Science and Engineering Discovery Environment (XSEDE) Open Science Grid (OSG) as the service provider. O.C. acknowledges the Brown University startup fund and the NSF fund (CBET-1936223).

REFERENCES

- (1) Kuo, W.-S.; Shao, Y.-T.; Huang, K.-S.; Chou, T.-M.; Yang, C.-H. ACS Appl. Mater. Interfaces 2018, 10, 14438.
- (2) Kang, S.; Kim, K. M.; jung, K.; Son, Y.; Mhin, S.; Ryu, J. H.; Shim, K. B.; Lee, B.; Han, H.; Song, T. Sci. Rep. 2019, 9, 4101.
- (3) Zebibula, A.; Alifu, N.; Xia, L.; Sun, C.; Yu, X.; Xue, D.; Liu, L.; Li, G.; Qian, J. Adv. Funct. Mater. 2018, 28, 1703451.
- (4) De Liberato, S. Nat. Photonics 2018, 12, 4.
- (5) Samuel, I. Nat. Mater. 2018, 17, 9.
- (6) Li, Y.; Hou, X.; Dai, X.; Yao, Z.; Lv, L.; Jin, Y.; Peng, X. J. Am. Chem. Soc. 2019, 141, 6448.
- (7) Mei, S.; Liu, X.; Zhang, W.; Liu, R.; Zheng, L.; Guo, R.; Tian, P. ACS Appl. Mater. Interfaces 2018, 10, 5641.
- (8) Wu, K.; Li, H.; Klimov, V. I. Nat. Photonics 2018, 12, 105.
- (9) Wang, W.; Feng, W.; Du, J.; Xue, W.; Zhang, L.; Zhao, L.; Li, Y.; Zhong, X. Adv. Mater. 2018, 30, 1705746.
- (10) Zhou, Y.; Zhao, H.; Ma, D.; Rosei, F. Chem. Soc. Rev. 2018, 47, 5866.
- (11) Bai, F.; Bian, K.; Huang, X.; Wang, Z.; Fan, H. Chem. Rev. 2019, 119, 7673.
- (12) Kelley, M. L.; Letton, J.; Simin, G.; Ahmed, F.; Love-Baker, C. A.; Greytak, A. B.; Chandrashekhar, M. V. S. ACS Appl. Electron Mater. 2020, 2, 134.
- (13) García-Santamaría, F.; Brovelli, S.; Viswanatha, R.; Hollingsworth, J. A.; Htoon, H.; Crooker, S. A.; Klimov, V. I. *Nano Lett.* **2011**, *11*, *687*.
- (14) Mahler, B.; Spinicelli, P.; Buil, S.; Quelin, X.; Hermier, J.-P.; Dubertret, B. *Nat. Mater.* **2008**, *7*, 659.
- (15) Reiss, P.; Protière, M.; Li, L. Small 2009, 5, 154.
- (16) Carbone, L.; Nobile, C.; De Giorgi, M.; Sala, F. D.; Morello, G.; Pompa, P.; Hytch, M.; Snoeck, E.; Fiore, A.; Franchini, I. R.; Nadasan, M.; Silvestre, A. F.; Chiodo, L.; Kudera, S.; Cingolani, R.; Krahne, R.; Manna, L. *Nano Lett.* **2007**, *7*, 2942.
- (17) Zhong, D.; Liu, W.; Tan, P.; Zhu, A.; Liu, Y.; Xiong, X.; Pan, J. Appl. Catal., B 2018, 227, 1.
- (18) Manna, L.; Milliron, D. J.; Meisel, A.; Scher, E. C.; Alivisatos, A. P. Nat. Mater. 2003, 2, 382.
- (19) Hamachi, L. S.; Yang, H.; Jen-La Plante, I.; Saenz, N.; Qian, K.; Campos, M. P.; Cleveland, G. T.; Rreza, I.; Oza, A.; Walravens, W.; Chan, E. M.; Hens, Z.; Crowther, A. C.; Owen, J. S. *Chem. Sci.* **2019**, *10*, *6539*.

- (20) Greytak, A. B.; Allen, P. M.; Liu, W.; Zhao, J.; Young, E. R.; Popović, Z.; Walker, B. J.; Nocera, D. G.; Bawendi, M. G. *Chem. Sci.* **2012**, *3*, 2028.
- (21) Geißler, D.; Würth, C.; Wolter, C.; Weller, H.; Resch-Genger, U. Phys. Chem. Chem. Phys. 2017, 19, 12509.
- (22) Tahara, H.; Sakamoto, M.; Teranishi, T.; Kanemitsu, Y. Nat. Commun. 2018, 9, 3179.
- (23) Leatherdale, C. A.; Woo, W. K.; Mikulec, F. V.; Bawendi, M. G. J. Phys. Chem. B **2002**, 106, 7619.
- (24) Dana, J.; Maity, P.; Jana, B.; Maiti, S.; Ghosh, H. N. ACS Omega **2018**, 3, 2706.
- (25) Xiao, S. J.; Zhao, X. J.; Chu, Z. J.; Xu, H.; Liu, G. Q.; Huang, C. Z.; Zhang, L. ACS Omega **2017**, 2, 1666.
- (26) Tessier, M. D.; De Nolf, K.; Dupont, D.; Sinnaeve, D.; De Roo, J.; Hens, Z. J. Am. Chem. Soc. 2016, 138, 5923.
- (27) Xu, J. X.; Vithanage, B. C. N.; Athukorale, S. A.; Zhang, D. Analyst 2018, 143, 3382.
- (28) Siriwardana, K.; Vithanage, B. C. N.; Zou, S.; Zhang, D. Anal. Chem. 2017, 89, 6686.
- (29) Athukorale, S. A.; Zhou, Y.; Zou, S.; Zhang, D. Anal. Chem. **2017**, 89, 12705.
- (30) Xu, J. X.; Yuan, Y.; Zou, S.; Chen, O.; Zhang, D. Anal. Chem. **2019**, 91, 8540.
- (31) Chen, Z.; Lei, Y.; Xu, H.; Chen, X.; Liu, J. J. Mater. Chem. B 2013, 1, 3031.
- (32) Guo, P.; Wang, Y.; Zhuang, Q. Sens. Actuators, B 2019, 299, 126873.
- (33) Zhang, L.-M.; Cui, Y.-X.; Zhu, L.-N.; Chu, J.-Q.; Kong, D.-M. *Nucleic Acids Res.* **2019**, 47, 2727.
- (34) Hou, Y.; Liu, J.; Hong, M.; Li, X.; Ma, Y.; Yue, Q.; Li, C.-Z. *Biosens. Bioelectron.* **2017**, 92, 259.
- (35) Xu, J. X.; Hu, J.; Zhang, D. Anal. Chem. 2018, 90, 7406.
- (36) Siriwardana, K.; Nettles, C. B.; Vithanage, B. C. N.; Zhou, Y.; Zou, S.; Zhang, D. *Anal. Chem.* **2016**, *88*, 9199.
- (37) Haes, A. J.; Zou, S.; Zhao, J.; Schatz, G. C.; Van Duyne, R. P. J. Am. Chem. Soc. **2006**, 128, 10905.
- (38) Yang, W.; Reed, J. M.; Wang, H.; Zou, S. Phys. Chem. Chem. Phys. 2010, 12, 12647.
- (39) Draine, B. T. Astrophys. J. 1988, 333, 848.
- (40) Draine, B. T.; Flatau, P. J. J. Opt. Soc. Am. A 1994, 11, 1491.
- (41) Chen, O.; Zhao, J.; Chauhan, V. P.; Cui, J.; Wong, C.; Harris, D. K.; Wei, H.; Han, H.-S.; Fukumura, D.; Jain, R. K.; Bawendi, M. G. *Nat. Mater.* **2013**, *12*, 445.
- (42) Jameson, D. M.; Ross, J. A. Chem. Rev. 2010, 110, 2685.
- (43) Collings, P. J.; Gibbs, E. J.; Starr, T. E.; Vafek, O.; Yee, C.; Pomerance, L. A.; Pasternack, R. F. *J. Phys. Chem. B* **1999**, *103*, 8474.
- (44) Xu, J. X.; Siriwardana, K.; Zhou, Y.; Zou, S.; Zhang, D. Anal. Chem. 2018, 90, 785.
- (45) Pietryga, J. M.; Park, Y.-S.; Lim, J.; Fidler, A. F.; Bae, W. K.; Brovelli, S.; Klimov, V. I. *Chem. Rev.* **2016**, *116*, 10513.